

REFERENCES AND NOTES

- J. F. Tull, *Geol. Soc. Am. Spec. Pap.* 191 (1982), p. 3; — and G. M. Guthrie, *Ala. Geol. Soc. Guideb. Annu. Field Trip* 22, 1 (1985).
- J. F. Tull et al., *Geol. Soc. Am. Bull.* 100, 1291 (1988).
- C. Butts, in *Geology of Alabama*, G. I. Adams, C. Butts, L. W. Stephenson, W. Cooke, Eds. (Geological Survey of Alabama, Tuscaloosa, 1926).
- T. J. Carrington, *Ala. Geol. Soc. Guideb. Annu. Field Trip* 11, 1 (1973); D. E. Sutley, thesis, University of Alabama (1977).
- The Erin was assigned originally a Carboniferous age (probably Pennsylvanian) on the basis of permineralized lycopsid (club moss) cones reported in the early twentieth century to have been recovered in the slates near the home of Joshua Franklin. E. A. Smith [*Science* 18, 244 (1903)] stated that "The general proportions and aspect of the cones are suggestive of some of the Carboniferous forms"; W. E. Prouty [*Pan Am. Geol.* 37, 365 (1922)] remarked that specimens identified "by David White proved without question the late Paleozoic and probable Carbonic age"; D. White [communication to C. Butts in (3), p. 219], assigned "all probability of Carboniferous and probably of Pennsylvanian age"; R. A. Gastaldo and R. B. Cook [*Geol. Soc. Am. Spec. Pap.* 191 (1982), p. 69] concurred with the Carboniferous age assignment because of the level of strobilar development exhibited by the lycopsid cones.
- J. F. Tull, in *The Caledonides in the USA*, D. R. Wones, Ed. (Department of Geological Sciences, Virginia Polytechnic Institute and State University, Blacksburg, 1980), pp. 167–177; G. M. Guthrie, *Ala. Geol. Surv. Bull.* 131, 1 (1989); *ibid.*, in press.
- S. A. Kish, *Geology* 18, 650 (1990).
- J. W. Mies, *Ala. Geol. Surv. Bull.* 148, 1 (1992); G. M. Guthrie, unpublished data.
- W. E. Osborne, M. W. Szabo, T. L. Neathery, C. W. Copeland Jr., *Ala. Geol. Surv. Spec. Map* 220 (1988).
- J. F. Tull et al., *Geol. Soc. Am. Abstr. Programs* 21, 342 (1989).
- Collection 121388 was made on 13 December 1988 by R. B. Cook and graduate students. Specimen 121388.1 was collected by T. M. Demko from the type section of the Erin Slate on the north side of the railroad cut (NE1/4, NW1/4, sec. 28, T19S, R7E, Clairmont Springs 7.5-min quadrangle). Collections 61091 to 61291 were made between 10 to 12 June 1991 by R. A. Gastaldo and G. M. Guthrie from the same outcrop and from float exposed in a field to the east of the improved road [E1/2, SW1/4, sec. 21, T19S, R7E, Clairmont Springs 7.5-min Quadrangle]. Specimen 61091.35 was collected by R. A. Gastaldo from the type section of the Erin, located above. Collection 7991 was made on 9 July 1991 by R. A. Gastaldo, M. Smith, and M. Ebbert from the field east of the road, located above.
- Samples of organic-rich elliptical-elongate structures and carbonaceous rinds of permineralized plant fossils were analyzed by Rock-Eval pyrolysis at the Institut Français du Pétrole (IFP nos. 121388.1 and 121388.16; A. Y. Huc, written communication).
- Low-grade metamorphism results in organic matter with high contrast. Therefore, photographs were made with Kodak TMax film and a 50-mm macroscopic lens fitted with various black and white filters on an Olympus OM-1 camera. Specimens, glass side up, were illuminated with a True-View Light Box (Logan Specialty) located beneath.
- F. Unger, *Kongl. Akad. Wiss. Wien. Denkschr.* 11, 139 (1856); C. B. Beck, *Am. J. Bot.* 65, 221 (1978); D. H. Scott and E. C. Jeffrey, *Philos. Trans. R. Soc. London Ser. B*, 205, 315 (1914); J. Galtier, written communication; F. Hueber, written communication. Detailed specimen descriptions can be found in R. A. Gastaldo, *J. Paleontol.*, in press.
- C. B. Read, *J. Paleontol.* 10, 215 (1936); A. T. Cross and J. H. Hoskins, *ibid.* 25, 713 (1951); J. E. Conkin and B. M. Conkin, in *Devonian-Mississippian Boundary in Southern Indiana and Northwestern Kentucky*, J. E. Conkin and B. M. Conkin, Eds. (9th International Congress of Carboniferous Geology and Stratigraphy, Urbana, IL, 1979); F. Ettensohn et al., in *Devonian of the World*, N. J. McMillan, A. F. Embry, D. J. Glass, Eds. (Canadian Society of Petroleum Geology, Calgary, 1988), pp. 323–345; T. L. Robl and L. S. Barron, *ibid.*, pp. 377–392.
- J. Galtier and B. Meyer-Berthaud, *Palaeontogr. Abt. B* 213, 1 (1989).
- , N. P. Row, *Cour. Forsch. Inst. Senckenberg* 100, 109 (1988).
- G. M. Guthrie and D. E. Raymond, *Ala. Geol. Surv. Bull.* 150, 1 (1992).
- Kish (7) reported K-Ar ages that range from 425 to 322 million years ago (Ma). To arrive at a Devonian age for regional metamorphism, he calculated an average age of 399 ± 17 Ma using all but the youngest age (329 ± 7 Ma) determination. He then argued that because the cleavage-forming event affected rocks containing Early Devonian fossils, it must be of at least Early Devonian age. The acquisition of spurious conventional K-Ar ages on slates has been well documented (R. P. Wintsch, M. J. Kunk, J. B. Epstein, *Am. J. Sci.*, in press) and may be the result of extraneous fractions of argon trapped in crystals or the incorporation of detrital or diagenetic grains or one or more generations of white mica that formed from one or more cleavage-forming assemblages.
- R. Unrug and S. Unrug, *Geol. Soc. Am. Abstr. Programs* 18, 1041 (1990).
- , S. L. Palmes, in *Studies of Precambrian and Paleozoic Stratigraphy in the Western Blue Ridge*, S. A. Kish, Ed. (Carolina Geological Society, 1991), pp. 27–38.
- T. W. Broadhead, R. D. Hatcher Jr., J. O. Costello, *ibid.*, pp. 39–44; D. Walker and N. Rast, *ibid.*, pp. 44–56.
- R. D. Dallmeyer, J. E. Wright, D. T. Secor, A. W. Snoko, *Geol. Soc. Am. Bull.* 97, 1329 (1986); J. W. Horton, J. F. Sutter, T. W. Stern, D. J. Milton, *Am. J. Sci.* 287, 635 (1987).
- M. G. Steltenpohl, S. A. Goldberg, T. B. Hanley, M. J. Kunk, *Geology* 20, 845 (1992); M. G. Steltenpohl and M. J. Kunk, *Geol. Soc. Am. Bull.* 105, 819 (1993).
- M. W. Higgins and I. Zietz, *Geol. Soc. Am. Mem.* 158, 125 (1983); H. Williams and R. D. Hatcher Jr., *Geology* 10, 530 (1982); *Geol. Soc. Am. Mem.* 158, 33 (1983); J. W. Horton, I. Zietz, T. L. Neathery, *Geology* 12, 51 (1984).
- R. D. Dallmeyer, *Am. J. Sci.* 289, 812 (1989).
- K. D. Nelson et al., *Geology* 13, 714 (1985); F. A. Cook, L. Brown, J. E. Oliver, T. Petersen, *Geol. Soc. Am. Bull.* 92, 161 (1981).
- D. T. Secor, A. W. Snoko, R. D. Dallmeyer, *Geol. Soc. Am. Bull.* 97, 1345 (1986); R. D. Hatcher Jr., W. A. Thomas, G. Viele, *The Appalachian-Ouachita Orogen in the United States* (Geological Society of America, Boulder, CO, 1990).
- R. D. Hatcher Jr., *Annu. Rev. Earth Planet. Sci.* 15, 237 (1987); J. W. Horton Jr., A. A. Drake Jr., D. W. Rankin, *Geol. Soc. Am. Spec. Pap.* 230 (1989), p. 213.
- Supported by National Science Foundation grant EAR 9019286 (R.A.G.) and American Chemical Society, Petroleum Research Fund, grant 23762-GB2 (M.G.S.).

25 May 1993; accepted 1 September 1993

Structure at 2.5 Å of a Designed Peptide That Maintains Solubility of Membrane Proteins

Christian E. Schafmeister,* Larry J. W. Miercke, Robert M. Stroud

A 24-amino acid peptide designed to solubilize integral membrane proteins has been synthesized. The design was for an amphipathic α helix with a "flat" hydrophobic surface that would interact with a transmembrane protein as a detergent. When mixed with peptide, 85 percent of bacteriorhodopsin and 60 percent of rhodopsin remained in solution over a period of 2 days in their native forms. The crystal structure of peptide alone showed it to form an antiparallel four-helix bundle in which monomers interact, flat surface to flat surface, as predicted.

The structures of integral membrane proteins are of interest to the field of structural biology, but they have been less than amenable for determination by x-ray crystallography. Crystals of at least 20 membrane proteins have been obtained (1), but in only a few cases have the crystals been of suitable quality to permit the resolution of atomic structure (2). With the hypothesis that small-molecule detergents, as required to solubilize membrane proteins, are in some way responsible for the disorder within the crystals (3), we attempted to design homogeneous peptides as detergents, "peptitergents" that would lead to a more homogeneous, well-ordered complex for crystallog-

raphy. Peptitergents are amphipathic peptides designed to sequester the hydrophobic membrane-spanning region of membrane proteins by packing around the protein in a rigid, well-ordered, parallel α -helical arrangement. The first peptitergent, PD₁, was designed, synthesized, and crystallized by itself and found to form an antiparallel four-helix bundle, a structure that is of interest from the point of view of de novo protein design. It also interacted with the integral membrane proteins bacteriorhodopsin and rhodopsin to maintain the majority of protein in solution for several days (Fig. 1). In contrast, PD₁ did not maintain PhoE porin solubility.

The peptide was designed as a 24-residue amphipathic α helix (Fig. 2) with a hydrophobic surface 30 Å in length, long enough to traverse the membrane-spanning region

Department of Biochemistry and Biophysics, University of California, San Francisco, CA 94143-0448.

*To whom correspondence should be addressed.

of an integral membrane protein. The hydrophobic surface was designed with alanines projecting from the center and leucines from the sides to form a wide, flat face that would permit interaction with the various surfaces of a transmembrane protein. The leucines were placed to allow them to interact with leucines on other PD₁ helices through hydrophobic contacts. Glutamic acid and lysine were used in an attempt to form salt bridges at the helix termini that would stabilize the helix termini; the salt bridges were designed to be at positions *i* and *i* + 4 and to be oriented so as to stabilize the helix dipole (4). The helix termini were capped by acetylation of the amino terminus and conversion of the carboxy terminus to an

amide to neutralize the potentially destabilizing terminal charges that would interact unfavorably with the helix dipole (5). Further stabilization of the helix dipole was attempted by the assignment of a glutamate as the second residue and a lysine as the second to last residue. Glutamine was used to fill the remaining positions on the hydrophilic face because of its hydrophilicity and helix-forming propensity (6). No aromatic residues were included because they are too bulky and hydrophobic.

The association of amphipathic helices to sequester hydrophobic groups from solvent is a feature of many natural helical coiled coils and four-helix bundles (7). Several groups have taken advantage of this phenomenon

to construct helical bundles as a first step along the path to de novo designed proteins (8, 9). It is this association between hydrophobic surfaces on helices that we exploited for association of peptitergents with transmembrane surfaces on membrane proteins and of peptitergent monomers with themselves. In solution, the PD₁ monomers were expected to dimerize flat surface to flat surface to bury the maximum hydrophobic surface area. The dimerization was expected to be antiparallel because the electrostatic interaction of the helix dipoles could dominate the overall interaction in the absence of "knobs into holes" packing. The dimers were expected to associate side to side through hydrophobic contacts of interdigitating leucines to form larger aggregates. These expectations were borne out by the x-ray crystal structure.

The structure of PD₁ was determined by molecular replacement (Tables 1 and 2). A Fourier transform of the intensities showed a strong peak, one-quarter of the height of the origin peak, at $5.2 \pm 0.2 \text{ \AA}$ along the crystallographic *c* axis; this is characteristic of α -helical structure and indicated that helices are oriented with their long axes nearly parallel to the *c* axis (10). Molecular replacement was applied with a single, 24-residue polyalanine α helix as the search molecule. For the best orientation of the search helix, difference density maps revealed peaks for several fully occupied leucines. Of the 20 nonalanine side chains, 16 were built during 16 cycles of model building and difference map refinement (11), revealing the details of the hydrophobic core, crystal contacts, and several ordered glutamines near hydrophobic residues. The structure was refined to 3.0 \AA resolution to an R_{factor} of 19.6% and to 2.5 \AA with an

Table 1. Crystallization and data-collection parameters. Crystallization of PD₁ occurs at room temperature in 45 to 60% saturated ammonium sulphate, a 5.5 mg/ml solution of PD₁, and 0.1 M tris (pH 7.5) in hanging drops by vapor diffusion. There are two crystal forms: the more common long hexagonal rods (form I), 400 μm by 75 μm , and large, irregular crystals (form II), 1.5 mm by 500 μm . Form I crystals dissolve easily, presumably because of temperature fluctuations; thus, image plate data were collected with form II crystals on a Rigaku Raxis IIC.

Parameter	Value
Observations (no.)	14,611
Unique observations $F > 2\sigma$ (no.)	1,186
Unique observations $F > 4\sigma$ (no.)	829
Overall completeness (%)	97
R_{merge}^*	5.8
<i>a</i> , <i>b</i> (\AA)	41.0
<i>c</i> (\AA)	67.1

* $R_{\text{merge}} = (\sum |I_i - \langle I_i \rangle|) / \sum I_i$, where $\langle I_i \rangle$ is an average of I_i over all symmetry related reflections.

Fig. 1. Percent solubilization of (A) bacteriorhodopsin (BR) and (B) rhodopsin (Rho) by the peptitergent PD₁. For PD₁ samples, concentrated protein was added to dry peptide (100:1 molar ratio of PD₁ to protein) with stirring followed by the addition of buffer to obtain 100-fold dilution. All samples were prepared and stored at 4°C. Extent of solubilization was determined by an assay of total protein concentration (unfilled symbols) and by optical density (filled symbols) at 500 nm for Rho and 550 nm for BR after ultracentrifugation (60 min at 219,000g). Total protein was determined by a Lowry assay in the presence of SDS (22) with the following changes: sample volume was 0.1 ml; 1.0 ml of reagent C (22) was added followed by addition of 0.1 ml of dilute phenol reagent. (A) Concentrated, delipidated BR: 5 mg per milliliter of solution in 18 mM nonyl-glucoside (NG) (23), diluted 100-fold with BR buffer (5 mM sodium acetate, pH 5) in the presence of PD₁ (triangles) or with BR buffer containing 18 mM NG (circles). (B) Concentrated Rho: 3 mg/ml in 10 mM lauryldimethylamine oxide (LDAO), diluted with Rho buffer (10 mM potassium phosphate, pH 7) in the presence of PD₁ (triangles) or with Rho buffer containing 10 mM LDAO (squares). The Rho-LDAO mixed micelles were prepared by concanavalin A affinity chromatography (24) with the following modifications: rod outer segments (26 mg of Rho/ml) was solubilized in 200 mM CHAPSO and chromatographed using 16 mM CHAPSO. CHAPSO was exchanged for LDAO by multiple high-pressure ultrafiltration steps (23), concentrated to ~10 mg/ml and dialyzed for 7 days against 10 mM LDAO, 50 mM KPO₄, pH 7.

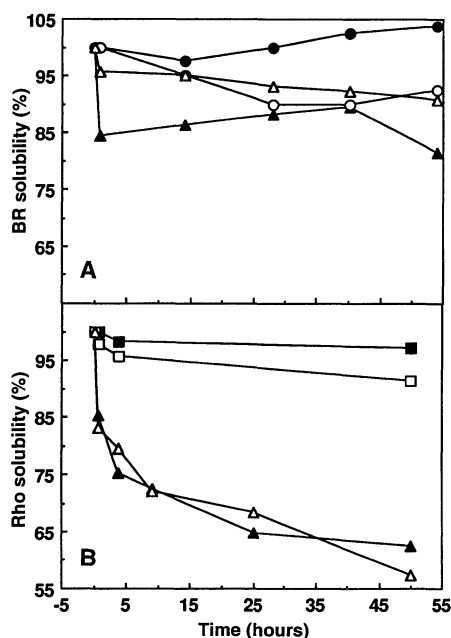
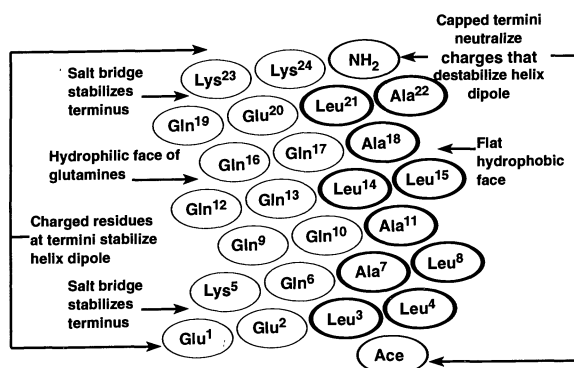


Fig. 2. Illustrative helical net diagram of the peptide sequence. The sequence reads NH₂- to COOH-terminus up the page to correspond to the orientation of helix I in other figures. The peptide sequence was synthesized with t-Boc (t-Butoxycarbonyl protection) chemistry on an ABI 431A solid-phase peptide synthesizer at standard scale (0.5-mmol resin). Purification was done on a Vydac C₁₈ (300 \AA pore, 5- μm particles) reverse phase column. Mass spectroscopy showed the correct molecular ion peak at 2819. Circular dichroism showed the peptide to have α -helical structure ($[\theta]_{222} = -10,200 \text{ cm}^2 \text{ deg}^{-1} \text{ mol}^{-1}$ at less than 600 μM , 20°C, pH 7.0). The solubility is greater than 10 mg per milliliter of water.



R_{factor} of 21.0% with 90% of the atoms built into density (Table 2). Simulated annealing omit maps of the leucine side chains invariably produced density peaks with a difference greater than 3σ at the expected sites (Fig. 3).

The left-handed super-coiled PD₁ four-helix bundle is formed by the single helix and three others related by 222 symmetry. The bundle is about 35 Å by 20 Å (Fig. 4A) with the long dimension of the bundle lying parallel to the crystallographic *c* axis. The interface between helices I and II (and III

Table 2. Refinement and refinement statistics. The determination of the crystal structure was achieved by molecular replacement, starting with a model of a 24-residue polyalanine α helix. All calculations and searches were done with X-PLOR (21). There is one peptide per asymmetric unit. A rotation search generated 40 solutions, which were all nearly coaxial, rotated away from the *c* axis by about 13°. The rotation solutions were subjected to rigid-body refinement, and the best solution was subjected to four translation searches; two space groups were searched, $P6_22$ and $P6_422$, each with the two orientations of helix up and helix down. Each translation search generated a single cluster of solutions within 1% of the volume of the unit cell. The top 200 solutions of each search were subjected to rigid-body refinement and used for finer searches around the helix axis that located the lowest R_{factor} solution of 47% in space group $P6_422$. Initial difference density maps showed positive peaks greater than 3σ , which were interpreted as leucines number 4, 8, and 21. Data to 3.0 Å was used, and a random 10% of the diffraction data were set aside to calculate R_{free} (25). Sixteen iterative cycles of adjustment against the difference maps (11) were carried out with CHAIN (26). Finally, 50 cycles of positional refinement and refinement of group *B* factors (one *B* factor for each residue main chain and another for each side chain) were performed, which reduced the R_{factor} from 49.1 to 19.6% and R_{free} from 42.5 to 26.0% for data between 7.5 and 3.0 Å (R_{factor} of 21.0% and an R_{free} of 25.9% for data from 7.5 to 2.5 Å). One 3σ peak in the difference maps that persisted through several cycles of refinement and was within 3.0 Å of three hydrogen-bonding groups was interpreted as an ordered water molecule. Simulated annealing from 4000 to 300 K in 150 steps following omission of individual side chains produced appropriate positive difference density peaks at the expected sites providing conformation of their location.

Refinement parameter	Value
Reflections (no.)	981
Parameters (no.)	582
Protein atoms included (no.)	178
Protein atoms missing (no.)	20
Waters added (no.)	1
Root-mean-square deviations from ideal	
bond lengths (Å)	0.02
bond angles (degrees)	2.8
torsions (degrees)	18.8

$$^*R_{\text{factor}} = (\sum |F_{\text{obs}}| - |F_{\text{calc}}|) / \sum |F_{\text{obs}}|$$

and IV) is the contact between the flat surface of helix I and the flat surface of helix II, with a helix-axis separation of 9.0 Å and a crossing angle of -20° . The interface between helices I and IV (and II and III) is through interdigitating leucines (Fig. 4B) and is characterized by a helix-axis separation of 10.1 Å and a crossing angle of -18° . The PD₁ helix has two sides, described by the sequence numbers of the leucines projecting from each side. Leucines 4, 8, and 15 are on the side that is buried within the core of the four-helix bundle and that forms the interdigitating leucine-helix contacts. Leucines 3, 14, and 21 are on the outside of the bundle; leucines 3 and 21 are buried within the crystal contact between the bundles, and leucine 14 is partially exposed to solvent and partially buried by the ordered glutamine 10. At the center of the bundle there is a hydrophobic cavity with a volume of $\sim 60 \text{ \AA}^3$ that does not contain electron density for solvent (12).

The average *B* factor for all atoms built into electron density on residues 3 through 21 is 68 Å²; alanine 11 has the lowest *B* factor of 29 Å². These values are unusually high; however, they are entirely consistent with the overall Wilson *B* factor of 76 Å² for the data, indicative of thermal and positional disorder within the crystal. In the context of the average *B* factor of 68 Å², the electron content of side chains with high *B* factors on this order are still seen unequivocally with full occupancy (11). There is no direct evidence for the formation of the salt bridges that were designed to stabilize the termini and helix dipole; the lysine side chains were too disordered to see in density maps. The first two and last three residues were disordered and their group *B* factors were much larger than the average, suggesting that the termini are partially

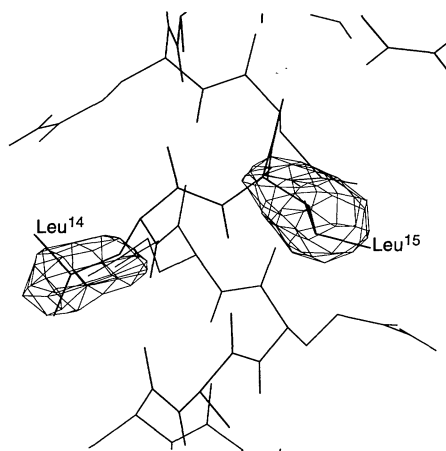


Fig. 3. $|F_{\text{obs}}| - |F_{\text{calc}}|$ simulated annealing omit map of leucines 14 and 15. Leucine side-chain occupancies were set to zero and the model was slowly cooled from 4000 to 300 K in 150 steps. The map is contoured at 3σ .

unraveled. Positive difference density could be seen for all glutamine side chains that protrude directly into solvent; however, there often was no single rotamer that best fit the density. These side chains had group *B* factors that refined to values greater than 100 Å², indicating that they occupy several conformations. Leucines and alanines within the hydrophobic core had very clear density and had group *B* factors that refined to relatively lower values. Essentially, the bundle appears to be ordered around the hydrophobic core.

The PD₁ four-helix bundle shares features with natural four-helix bundles; the crossing angle of -20° is characteristic of the type III helix interaction (13) seen in the proteins hemerythrin and cytochrome *c'* (7, 14). This crossing angle is reminiscent of a coiled-coil structure; however, the PD₁ helices are straight and have 3.6 residues per helical turn. This crossing angle is also seen in the synthetic three-helix bundle of another designed α helix, named "coil-Ser" (9). The total surface area buried within the PD₁ bundle is about 4200 Å² (15), $\sim 1050 \text{ \AA}^2$ per helix. This is comparable to the $\sim 1300 \text{ \AA}^2$ of surface for each helix that is buried within the coil-Ser three-helix bundle, although the coil-Ser hydrophobic surface is about one helix turn longer.

The primary goal is to solvate integral membrane proteins for crystallization. The integral membrane proteins bacteriorhodopsin (BR) (16) and bovine rhodopsin (Rho) (17) are good systems for a test of solubilization because the visible absorption spectra associated with the bound chromophore retinal are especially sensitive to their environment and allow quantitation. To test the solubility properties of membrane proteins by PD₁, we diluted purified BR in nonyl-glucoside (NG) and purified Rho in lauryldimethylamine oxide (LDAO) so that the detergent concentrations were less than 1/20 of their critical micellar concentrations (CMC); dilution was followed by ultracentrifugation. This was done both in the absence of PD₁, where the protein is 100% insoluble, and in the presence of PD₁ as follows. Delipidated BR solubilized in 18 mM NG, diluted to a final concentration of 180 μM NG in the presence of a final concentration of 200 μM PD₁ (PD₁ monomer to BR ratio of 100:1), gave an initial loss of less than 15% insoluble protein with no further loss after 2 days (Fig. 1A). When Rho in 10 mM LDAO was diluted with PD₁ identically to BR above, Rho slowly precipitated leaving about 60% soluble after 2 days (Fig. 1B). PD₁ must maintain complete stability of both these retinal-containing proteins because all protein remaining in solution was correctly folded, as shown by the optical density of the bound retinal (Fig. 1). Furthermore, there is no change in tertiary structure; in the presence of PD₁ or detergent, the

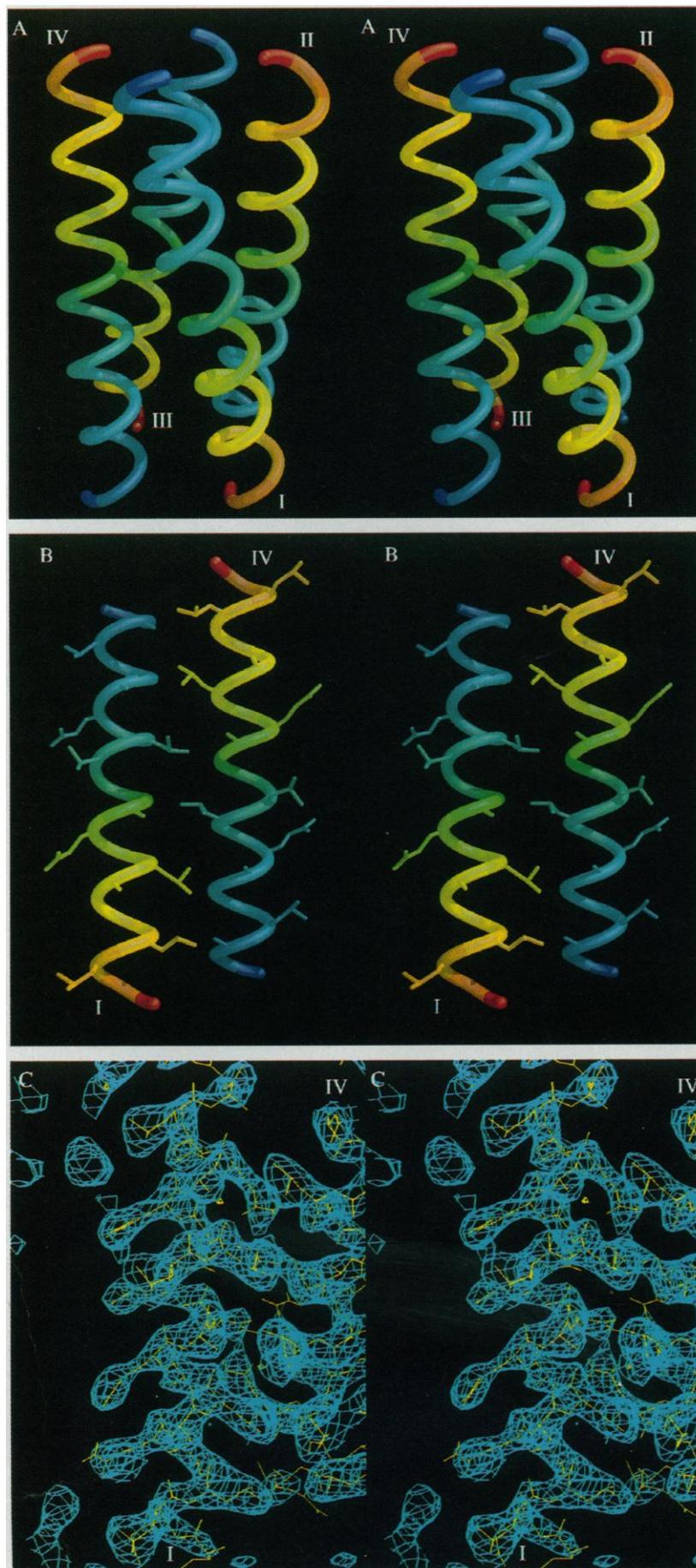
Fig. 4. Structure of the PD₁ four-helix bundle. **(A)** Four-helix bundle side view. The NH₂-terminus is red and the COOH-terminus is blue (9). The helices are labeled I, II, III, and IV to correspond to the descriptions in the discussion. **(B)** Cut-away side view of helices I and IV. View from within the hydrophobic core. Helices II and III have been removed to reveal the flat surface formed by each helix and the interdigitating leucines between helices I and IV. On helix I, from bottom to top, the interdigitating residues are leucines 4, 8, and 15. **(C)** $2|F_o| - |F_c|$ map for the entire helix. All of the density for helix I, seen from within the hydrophobic core. The map was contoured at 1.5σ .

visible absorption spectra are identical. The final concentration of NG and LDAO was about 1/36 and 1/22 of their CMC values, respectively [NG CMC = 6.5 mM (18), LDAO CMC = 2.2 mM (19)]. When diluted without detergent or PD₁, both proteins gave 100% precipitation. In contrast, PhoE porin (20) in 50 mM octyl glucoside completely precipitated when diluted with PD₁ or with buffer, without detergent. Thus, not all membrane proteins are solubilized by this particular peptide design. Porin is an all- β sheet structure, whereas BR and Rho are all helical and may thus interact differently.

Peptitergents can be redesigned, synthesized, and tested for individual solubilization properties tailored to particular membrane proteins. Their homogeneity and the variation in their properties possible through sequence variation may make them novel alternatives to small-molecule detergents for the solubilization and crystallization of integral membrane proteins.

REFERENCES AND NOTES

1. W. Kühlbrandt, *Q. Rev. Biophys.* **21**, 429 (1988).
2. J. Deisenhofer, O. Epp, K. Miki, R. Huber, H. Michel, *Nature* **318**, 618 (1985); M. S. Weiss *et al.*, *Science* **254**, 1627 (1991).
3. M. Zulauf, in *Detergent Phenomena in Membrane Protein Crystallization: Crystallization of Membrane Proteins*, H. Michel, Ed. (CRC Press, Boca Raton, FL, 1988), pp. 53–72; H. Michel, *ibid.*, pp. 73–88; R. M. Garavito *ibid.*, pp. 89–105.
4. S. Marqusee and R. L. Baldwin, *Proc. Natl. Acad. Sci. U.S.A.* **84**, 8898 (1987); M. F. Perutz and G. Fermi, *Proteins* **4**, 294 (1988).
5. K. R. Shoemaker, P. S. Kim, E. J. York, J. M. Stewart, R. L. Baldwin, *Nature* **326**, 563 (1987); R. Fairman, K. R. Shoemaker, E. J. York, J. M. Stewart, R. L. Baldwin, *Proteins* **5**, 1 (1989); W. G. J. Hol, *Prog. Biophys. Mol. Biol.* **45**, 149 (1985).
6. G. Casari and M. J. Sippl, *J. Mol. Biol.* **224**, 725 (1992); K. T. O'Neil and W. F. DeGrado, *Science* **250**, 646 (1990).
7. S. R. Presnell and F. E. Cohen, *Proc. Natl. Acad. Sci. U.S.A.* **86**, 6592 (1989).
8. L. Regan and W. F. DeGrado, *Science* **241**, 976 (1988); M. H. Hecht, J. S. Richardson, D. C. Richardson, R. C. Ogden, *ibid.* **249**, 884 (1990); C. P. Hill, D. H. Anderson, L. Wesson, W. F. DeGrado, D. Eisenberg, *ibid.*, p. 543.
9. B. Lovejoy *et al.*, *ibid.* **259**, 1288 (1993).
10. F. H. C. Crick, *Acta Crystallogr.* **6**, 689 (1953).
11. J. L. Chambers and R. M. Stroud, *Acta Crystallogr. B* **33**, 1824 (1977).
12. We determined the cavity volume by constructing a molecular surface with a probe radius of 1.5 Å; F. M.



- Richards, *Annu. Rev. Biophys. Bioeng.* **6**, 151 (1977).
13. C. Chothia, M. Levitt, D. Richardson, *Proc. Natl. Acad. Sci. U.S.A.* **74**, 4130 (1977).
14. M. A. Holmes and R. E. Stenkamp, *J. Mol. Biol.* **220**, 723 (1991); B. C. Finzel, P. C. Weber, K. D. Hardman, F. R. Salemme, *ibid.* **186**, 627 (1985).
15. Calculations of accessible surface area were performed on X-PLOR (21) with a probe radius of 1.6 Å.
16. W. Stoekenius and R. A. Bogomolni, *Annu. Rev. Biochem.* **52**, 587 (1982).
17. M. L. Applebury and P. A. Hargrave, *Vision Res.* **26**, 1881 (1986).
18. W. J. De Grip and P. H. M. Bovee-Geurts, *Chem. Phys. Lipids* **23**, 321 (1979).
19. K. W. Herrmann, *J. Phys. Chem.* **66**, 295 (1962).
20. B. K. Jap and P. G. Walian, *Q. Rev. Biophys.* **23**, 367 (1990).
21. A. T. Brünger, J. Kuriyan, M. Karplus, *Science* **235**, 458 (1987).
22. M. A. K. Markwell, S. M. Haas, L. L. Bieber, N. E. Tolbert, *Anal. Biochem.* **87**, 206 (1978).
23. S. J. Milder, T. E. Thorgerisson, L. J. W. Miercke,

- R. M. Stroud, D. S. Kliger, *Biochemistry* **30**, 1751 (1991).
24. B. J. Litman, *Methods Enzymol.* **81**, 150 (1982).
25. A. T. Brünger, *Nature* **355**, 473 (1992).
26. J. Sack, *J. Mol. Graphics* **6**, 225 (1988).
27. We thank I. D. Kuntz and F. Cohen for helpful discussions, R. Cerpa for assistance in the peptide synthesis, A. Rice for the initial peptide purification, and B. Jap for providing purified PhoE porin. Mass spectrometry measurements were provided by the University of California, San Francisco (UCSF), Mass Spectrometry Facility (A. L. Burlingame, director), supported by the Biomedical Research Technology Program of the National Center for Research Resources (NCRR) [National Institutes of Health (NIH) NCRR BRTF 01614]. Molecular graphics images were produced with the Midas-Plus software system from the Computer Graphics Laboratory, UCSF. C.S. is a Howard Hughes Medical Institute predoctoral fellow. This work was supported by the NIH (GM24485).

1 June 1993; accepted 9 September 1993

Analysis of a Nucleoprotein Complex: The Synaptosome of $\gamma\delta$ Resolvase

Nigel D. F. Grindley

The $\gamma\delta$ resolvase protein is one of a large family of transposon-encoded site-specific recombinases. It performs recombination in a DNA-protein complex that contains 12 resolvase protomers and two copies of the 120-base pair DNA substrate, *res* (each with three binding sites for a resolvase dimer). A derivative of resolvase with altered DNA binding specificity was used to show that the role of resolvase at site I, which contains the crossover point, differs from its role at the other two binding sites. The resolvase dimers that initially bind to site I are the only ones that require the residue Ser¹⁰, essential for catalysis of DNA breakage. In addition, these site I-bound dimers do not use a specific interaction between dimers that is required elsewhere in the complex for synapsis of the *res* sites.

Large protein-DNA assemblies participate in DNA transactions such as transposition, site-specific recombination, and the initiation of replication (1). The DNA substrates often contain multiple binding sites for a protein that may function both as a structural component of the complex and as an enzymatic component, depending on its location in the complex. Examples of such assemblies include the transpososomes of phage μ and Tn7 (2), the intasome of phage λ (3), and the synaptosome of the resolvase family of site-specific recombinases (4, 5).

The $\gamma\delta$ resolvase protein (encoded by the $\gamma\delta$ transposon) carries out strand exchange within a synaptic complex that contains two 120-bp segments of DNA (known as *res*) and at least six dimers of resolvase (one dimer occupying each of the three binding sites that constitute *res*) (4, 5) (Fig. 1). The three binding sites within *res* are essential for its activity, and recombination occurs by DNA breakage and re-

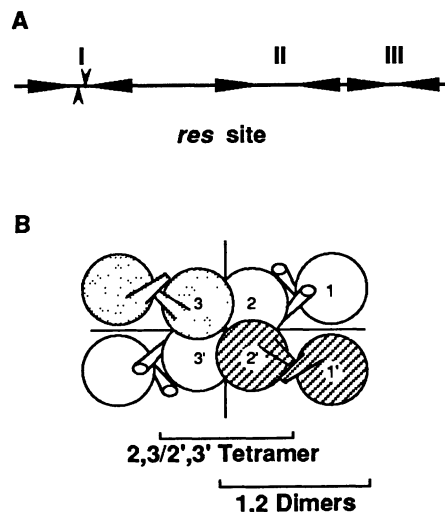
union at the center of site I. This synaptosome is a highly ordered structure—the two *res* sites are interwrapped, trapping precisely three negative superhelical turns (6)—and must be determined by a set of resolvase-

Fig. 1. Components of the synaptic complex assembled by $\gamma\delta$ resolvase. (A) The DNA substrate, *res* (~120 bp) contains three resolvase binding sites, indicated by the inverted pairs of arrowheads and labeled I, II, and III. The vertical arrowheads in the center of site I indicate the recombinational crossover point. (B) An assembly of eight resolvase catalytic domains showing the various inter-resolvase interactions seen in resolvase crystals (11, 17). Four 1,2 dimers are shown (two shaded, two white) with the crossed cylindrical projections representing the pair of COOH-terminal α helices that interact at the 1,2 interface. (The un-numbered domains form 1,2 dimers with those numbered 3 and 3'). Each dimer contributes one monomeric unit to the 2,3/2',3' tetramer at the center of the assembly. The COOH-terminal DNA binding domains are not shown (they are not visible in resolvase crystals) but would be attached to the ends of the COOH-terminal α -helical projections (17). The lines indicate two of the three orthogonal dyad axes.

DNA and resolvase-resolvase interactions constrained by the DNA linkage of the binding sites and by the negative superhelicity of the substrate. However, not all resolvase protomers in the complex are equal: only a subset provides catalytic function [defined here in the narrowest sense as providing the essential Ser¹⁰ residue that becomes covalently linked to the DNA during crossover site cleavage (4)], and it is likely that not all exhibit the same set of protein-protein interactions.

Our strategy for dissecting the structure and function of the synaptosome is to place specific mutants of resolvase—for example, those defective in chemical catalysis or in a defined set of protein-protein interactions—at specific binding sites within each *res* segment. The outcome of a resolution assay then indicates whether the resolvase bound at a defined site makes use of a specific protein-protein interaction during assembly of the synaptic complex or plays an active role in the chemical step of strand breakage. Specific binding to a mutant derivative of site I can be achieved with the resolvase mutant, R172L (with Arg¹⁷² replaced by Leu). This mutant was obtained by the use of a genetic screen (7) to select mutants of resolvase that could bind to a synthetic site I with a symmetrical G to T change at position 2 of the consensus half-site binding sequence TGTCCGATAATT (8).

We have used R172L to determine the location of the resolvase units that provide the active sites for catalysis of DNA breakage and reunion. The results of in vitro resolution reactions with pNG345 (a substrate containing the mutant site I^{G2T}) are shown in Fig. 2A (top panel). Two mutant resolvases were used: S10L, which lacks the critical Ser¹⁰ residue and binds weakly to site I (9), and R172L. S10L alone was



Department of Molecular Biophysics and Biochemistry, Yale University, Bass Center for Molecular and Structural Biology, New Haven, CT 06511.